

**"A Cochlear Nucleus Auditory  
Prosthesis based on microstimulation"**

Contract No. **No. NO1-DC-4-0005**  
Progress Report #12

**HUNTINGTON MEDICAL RESEARCH INSTITUTES**  
NEURAL ENGINEERING LABORATORY  
734 Fairmount Avenue  
Pasadena, California 91105

Douglas McCreery, PhD  
Martin Han, PhD

-----

-----  
**HOUSE EAR INSTITUTE**  
2100 WEST THIRD STREET  
Los Angeles, California 90057

-----  
R.V. Shannon, PhD  
Steve Otto, MS

## I: Work completed at HMRI

### Development of Multi-site Silicon Microelectrode Arrays

We have made considerable progress in the development of our second-generation multisite silicon probes. These probe profiles are shaped by deep reactive ion etching, which yields thick (100  $\mu\text{m}$ ) mechanically durable shanks.

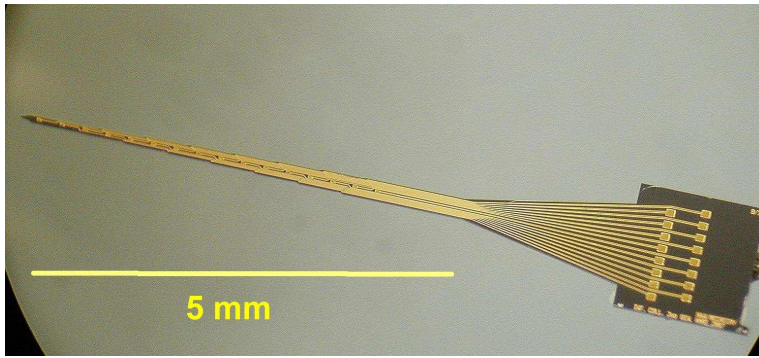
We are developing two probes; the “CN probe” is a 2-shank, 8-site stimulating probe for chronic implantation into the cat cochlear nucleus, but is intended to be a prototype for multisite probes in a clinical prosthesis. The “IC probe” is a single shank with 16 recording sites. It first will be used for acute recording of single and multi-unit activity in the central nucleus of the cat inferior colliculus (ICC), and then will be incorporated into an array that can be implanted chronically into the ICC by stereotaxis. The shape of the tip region and the rigidity of the shank are designed to allow these long (5 mm) probes to penetrate through the pia membrane covering the cat’s IC without bending or buckling, so that they can be implanted chronically through the cerebral hemisphere by stereotaxis. Their ability to easily penetrate through the pia over the IC has been verified in initial tests that will be described in the next quarterly report.

Based on our experience with the first-generation devices, the following major modifications have been implemented:

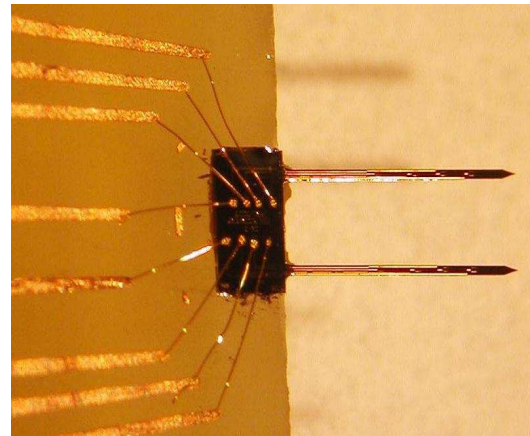
- (1) The conductive titanium-platinum-gold traces on the probes’ upper surface now are insulated with a triple sandwich of silicon dioxide-silicon nitride-silicon dioxide (ONO). The layers are deposited in succession by plasma-enhanced chemical vapor deposition (PECVD) in the clean room facility of the Nanoelectronics Research Facility (Nanolab) at the University of California at Los Angeles where excellent facilities to deposit low-stress films are available. (2) The electrode sites are being plated with electrodeposited iridium oxide (EIROF) to reduce the impedance of the IC recording probes and to increase the charge capacity of the CN stimulating probes. (3) The probes are now fabricated using silicon-on-insulator (SOI) wafers, instead of silicon wafers, to reduce variability in probe thickness during the “back-side” wafer processing (See Appendix). The thickness of the probes now is determined by the thickness of the wafer’s top “device” layer (100  $\mu\text{m}$  for the probes described in this report).
- (2) Several additional modifications have been made in the designs of the CN and IC probes: (i) The layout of the CN probes’ bonding pads has been changed so that a single probe design can be used for either side of a 2-probe array (See Figure 1e). (ii) The locations of the stimulating sites on the CN probes have been modified, based on recent animal experiments. (iii) The corners of probes have been rounded to reduce mechanical stress during handling. (iiii) Detachable tabs have been added to each probe to facilitate handling and mounting on the apparatus with which their tip regions are shaped. (v) Higher resolution photomasks have been manufactured by a new vendor. (vi) New printed circuit boards for electrical testing of the probes have been designed.

Details of the fabrication process are presented in the Appendix.

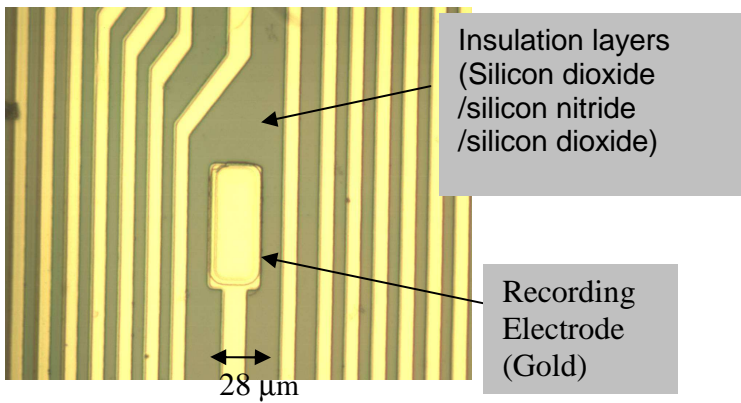
The new IC probe is shown in Figure 1a,b,c. Figure 1d shows the new CN probe mounted on a circuit board. The deep reactive ion etching process yields thick, mechanically sturdy probes, but with a vertical chisel-like tip. To facilitate passage through the pia and through the brain parenchyma with minimal disruption of brain tissue, the tip region is shaped by grinding against a surface charge with fine diamond particles (Figure 1c).



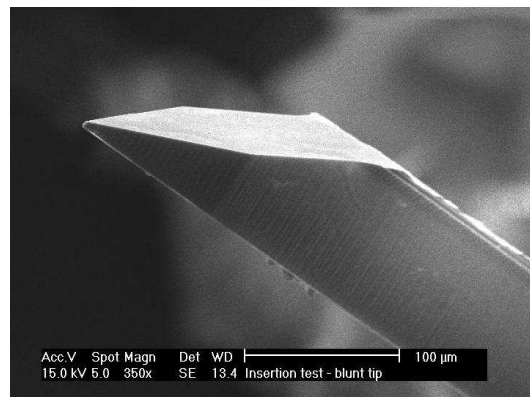
(a)



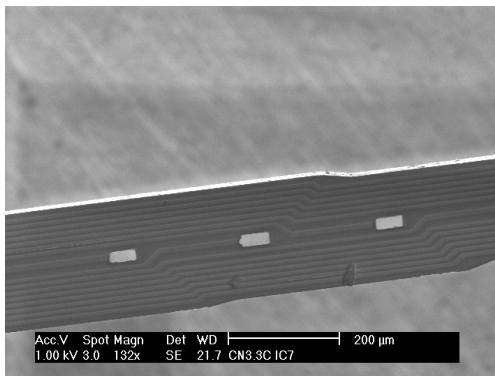
(d)



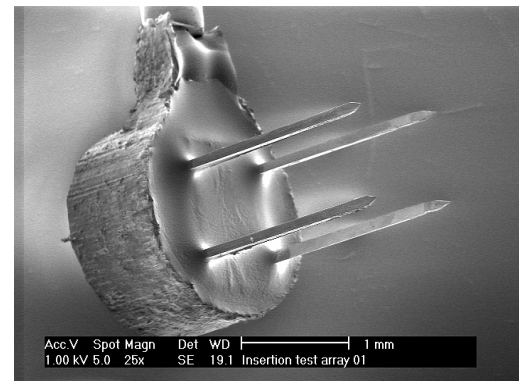
(b)



(e)



(c)



(f)

Figure 1: 2<sup>nd</sup> generation silicon probes fabricated by HMRI. (a) Scanning electron microscopic (SEM) view of a 100 μm-thick IC probe for recording in inferior colliculus. (b) Light-micrograph of a portion of the upper surface of the IC probe, showing one electrode site and the conductive traces. (c) A SEM of a portion of the IC probe. (d) A CN probe intended for implantation into the feline cochlear nucleus, mounted on a circuit board for soak-testing, (e) A SEM of the tip of a CN probe that has been sharpened by grinding and polishing against a surface charged with fine diamond particles. (f) An SEM of an array of two cochlear nucleus probes, in preparation for insertion testing into the feline spinal cord.

The CN probes are prototypes for an advanced central nervous system auditory prosthesis, and as such they must penetrate through the tough glia-pia membrane (glia limitans) that covers the human cochlear nucleus, without fracturing or chipping. Figure 1f shows an array of two CN probes that will be inserted into the feline spinal cord, using the hand-held inserter tool that is used to implant the prototype penetrating array into the cochlear nucleus of the human patients. The pia membrane near the dorsal root entry zone of the spinal cord lumbosacral enlargement is especially thick and difficult to penetrate with microelectrodes, and is our model of the glia limitans of the human brainstem. These insertion tests have begun and were successful with the first three arrays (arrays inserted into the cat spinal cord and removed with forceps, with no fractured shanks or chipped tips). The results of the entire series will be reported in full in the next quarterly report.

The electrode sites on both types of probes are being plated with electrodeposited iridium oxide (EIROF) in order to reduce the impedance of the IC recording probes and to increase the charge capacity of the CN stimulating probes. Figure 2a shows a representative plot of impedance vs. frequency of a site on the IC probe, in buffered saline, before and after plating with EIROF. The EIROF also greatly increases the sites' charge capacity which is essential for efficient microstimulation. This is illustrated in figure 2b.

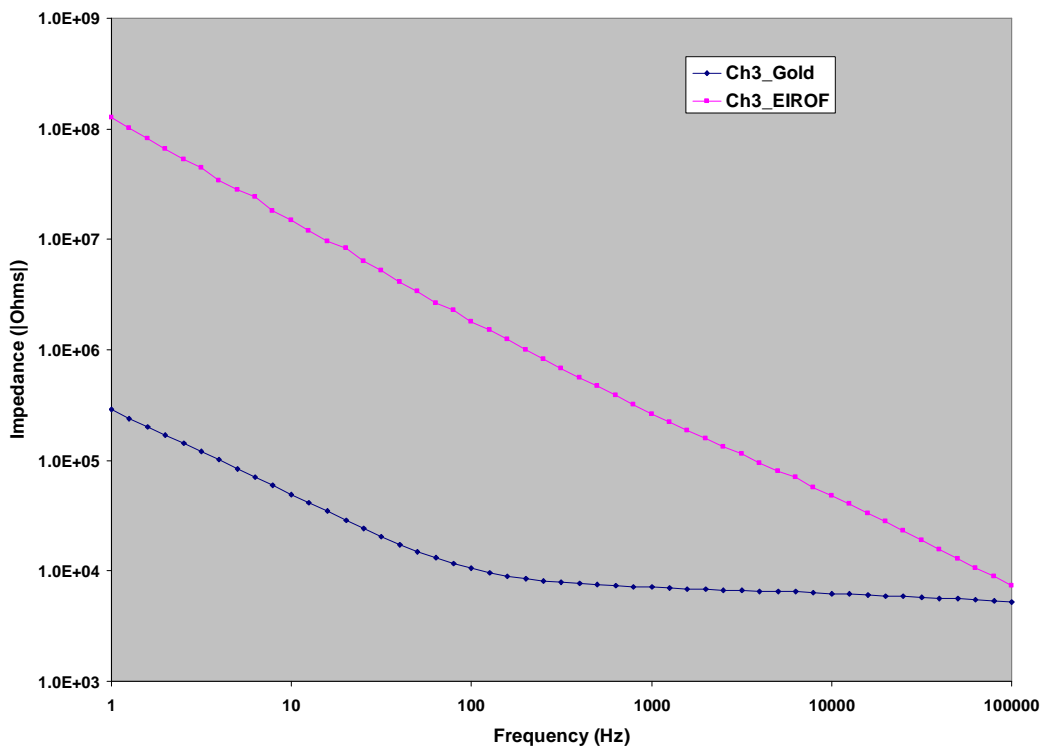


Figure 2A: Bode plots of the impedance of an electrode site in a HMRI-silicon probe before and after being electroplated with IrOx film (EIROF). The impedance measured in phosphate-buffered saline at 1 kHz was greatly reduced after electroplating IrOx onto the gold electrode sites (266 k $\Omega$  for gold (prior to electroplating) and 7.1 k $\Omega$  after plating). The surface area of the site was approximately 2,400  $\mu\text{m}^2$ .

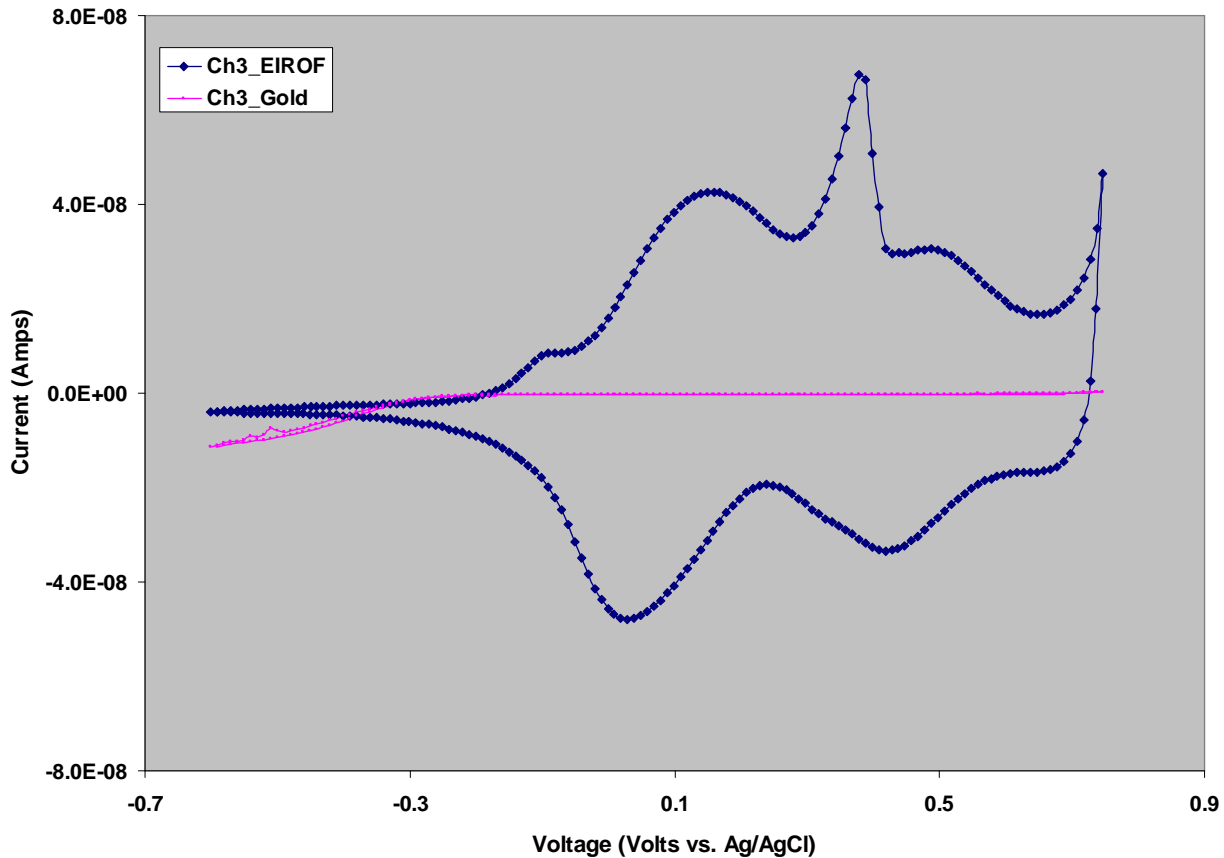


Figure 2B: Cyclic voltammograms of an electrode in a HMRI-silicon probe before and after being electroplated with IrOx film (EIROF), illustrating the large increase in charge storage capacities. The surface area of the site was approximately 2,400  $\mu\text{m}^2$ . Scan rate was 50 mV/sec.

We have begun soak-testing the probes in buffered saline, to detect either of two failure modes. First, the saline may come into contact with the gold conductive traces through flaws in the (outer) triple sandwich insulation. Such flaws may be present initially or may develop during prolonged saline soak due to degradation of the insulation. These flaws are detected by immersing the electrode site in saline, then continuing to slowly insert the remainder of the shank while monitoring the voltage transient induced by a small ( $\sim 5 \mu\text{A}$ ) biphasic current pulse. A sudden decrease in the amplitude of the voltage transient as the probe is advanced into the saline indicates that a flaw in the insulation has been immersed. The second possible failure mode is partial electrical shorting between certain channels due to intrusion of saline under the outer triple sandwich, either from the openings in the insulation at the electrode sites, or from the edges of the probe. This is detected and quantified by software that automatically generates an interchannel conductivity (“crosstalk”) matrix. A current pulse is injected into the saline through electrode site  $j$  and the amplitude of the voltage transient on all  $n$  channels is recorded, yielding an  $n \times n$  matrix that displays the normalized conductivity between all  $n^2$  pairs of sites. The conductivity between channels  $i$  &  $j$  is expressed as a percentage of the conductivity of channel  $i$  into the saline, with 0% indicating no conductivity between channels  $i$  and  $j$  and 100% indicating a complete short circuit. Thus the matrix of a probe for which there is no interchannel conductivity will show 0 at all off-diagonal positions and 100% on the main diagonal. Some minimal crosstalk (e.g., 1%) is generated by the sites’

common current path through the saline bath, but if there is no ongoing degradation, this should not increase during prolonged saline soak.

Three 2<sup>nd</sup> generation probes (one IC probe and two CN probes) were undergoing soak testing in buffered saline, for up to 17 days at the time of this report, and addition probes are being added. Figure 3a and 4b show the crosstalk matrices from a CN probe and an IC probe after 12 and 17 days in soak, respectively. There is no significant crosstalk between any of the channels. The tests for leaks in the insulating ONO triple sandwich are conducted at the same time as the crosstalk tests, and we have not detected flaws in the insulation of any of the probes.

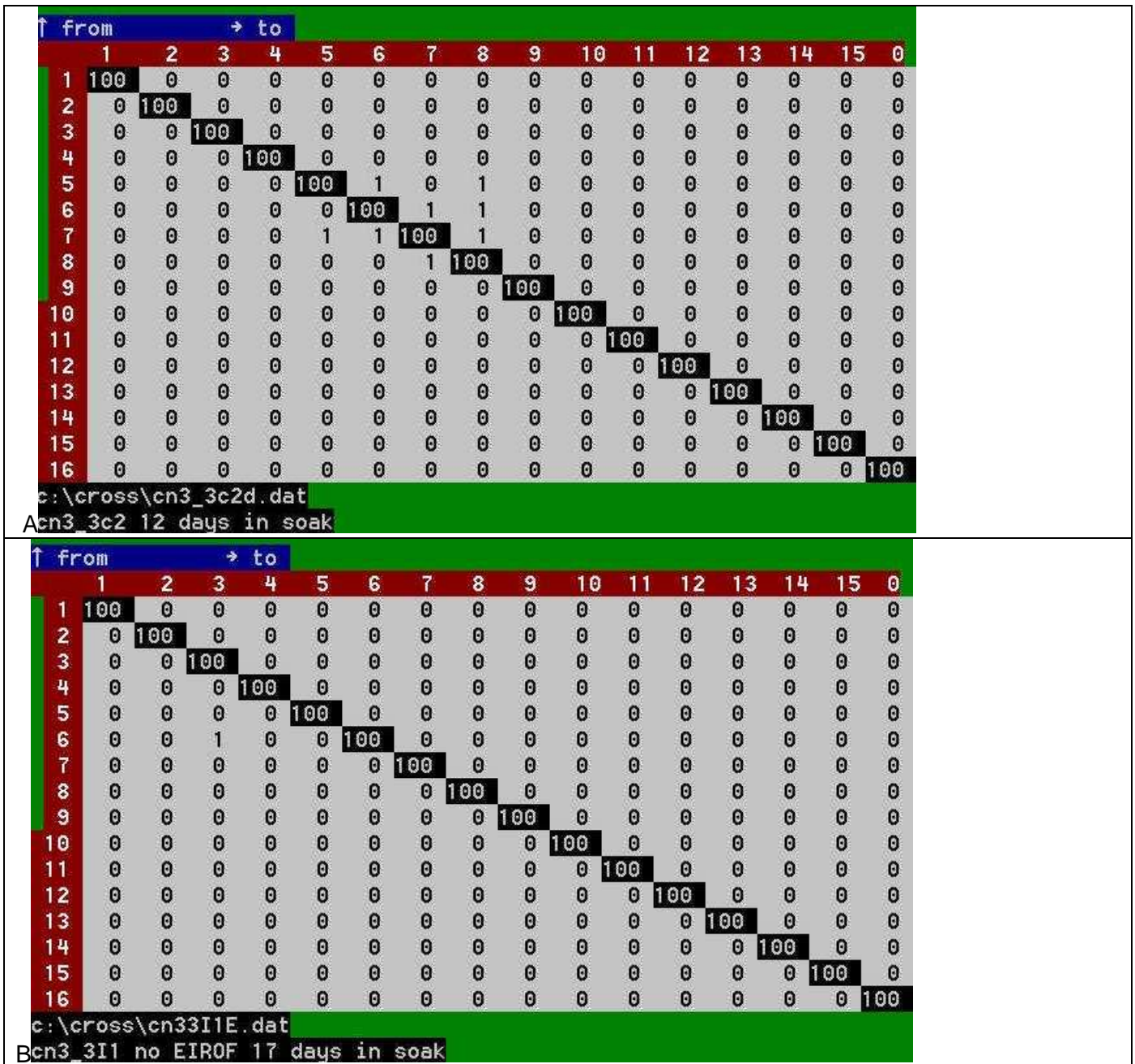


Figure 3. Crosstalk matrices of two 2<sup>nd</sup> generation CN probes undergoing soak tests in buffered saline. At 12 and 17 days, there is no significant conductivity between any channels.

Our soak-testing did reveal a problem with the electroplating process that must be remedied before these probes can be qualified for chronic implantation. Figure 4 shows the crosstalk matrix from an IC probe after 11 days in soak. There is significant conductivity (crosstalk) between 3 channels with adjacent traces (channels 2, 7 and 8). Examination of the probe by light microscopy revealed apparent intrusion of the EIROF film under the ONO sandwich, extending laterally from site 2 to the adjacent gold traces leading to sites 7 and 8. The EIROF was deposited onto each site in succession, using a potentiodynamic process in which a voltage of up to 0.8 volt, and thus a potential gradient of up to 50,000 volts/m was applied between the site being plated and the adjacent traces. We hypothesize that the EIROF film may have grown out along this gradient, wedging up the insulating ONO sandwich as it grew. If this is indeed what has occurred, it can be remedied by plating all of the sites simultaneously, so that there is no voltage gradient between the sites being plated and the adjacent conductive traces. In view of our considerable progress in the development of the 2<sup>nd</sup> generation probes during the last quarter, we are confident that this issue can be resolved without undue delay. Meanwhile, acute recording studies with the IC probes will commence.



Figure 5. Crosstalk matrix from an IC probe in which the electrode sites were plated with EIROF. There is significant crosstalk between channels 2, 7 and 8.

## Appendix – Details of the fabrication of the multisite probes

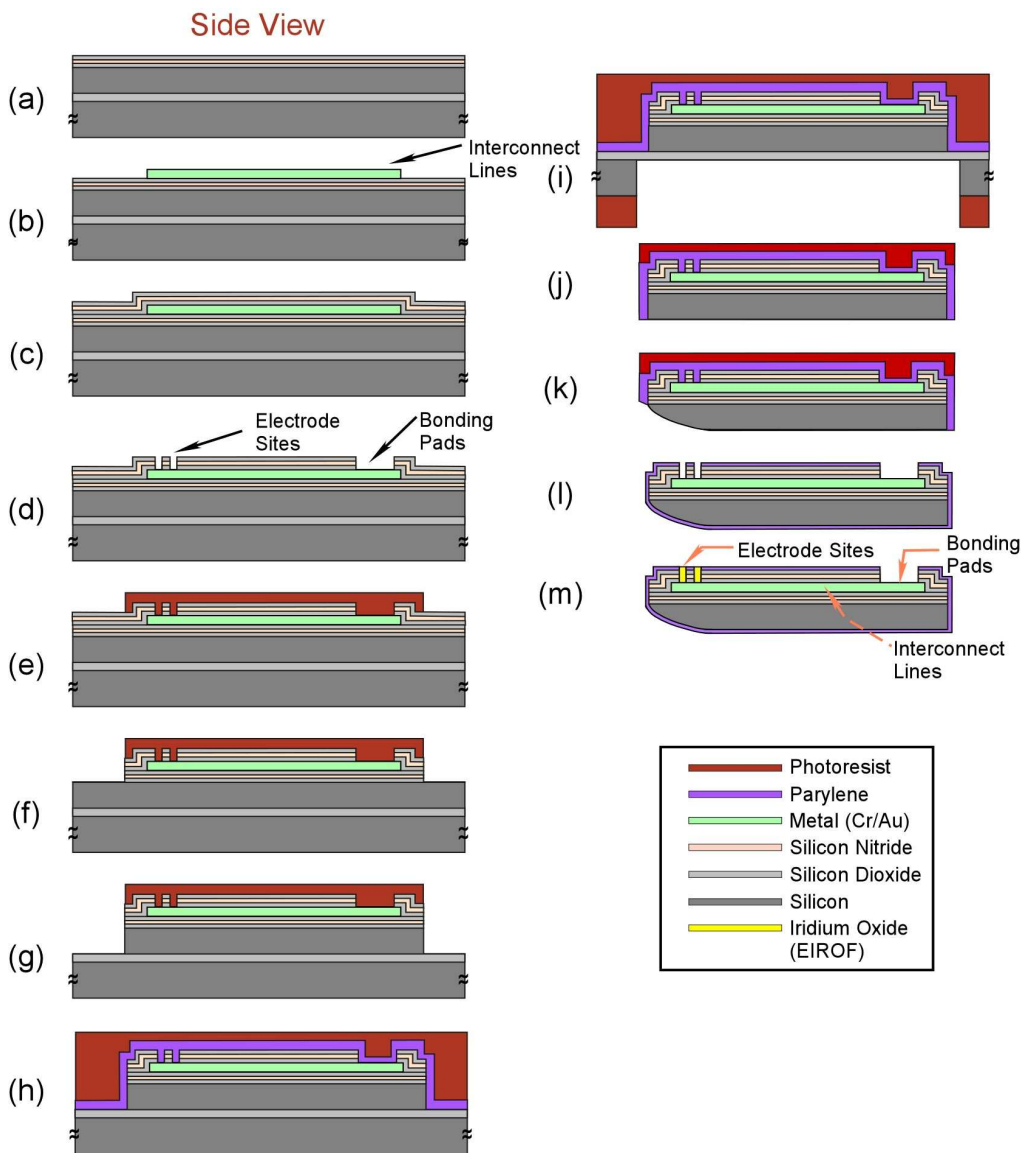


Figure A1: A process flow chart illustrating major steps involved in fabrication of HMRI-silicon probes. See texts for the details.

The major wafer-level fabrication steps are illustrated in Figure A1.

(a) On a silicon-on-insulator wafer, the first triple sandwich of silicon dioxide-silicon nitride-silicon dioxide (ONO) is deposited by PECVD (plasma-enhanced chemical vapor deposition). (b) A bilayer of photoresists (AZ 1518 and lift-off resist) is photolithographically patterned, and evaporation and lift-off of titanium, platinum and gold films are performed, defining the conductive traces between the bonding pads and the electrode sites. (c) The second ONO triple sandwich is deposited over the traces, to insulate them. (d) A layer of photoresist is spun onto the wafer and patterned by photolithography. Then, buffered hydrofluoric acid is used to etch the ONO layers to open windows to the recording/stimulating

sites and bonding pads. (e) A thick photoresist layer (AZ4400) is spun onto the wafer and is patterned to define the shape of the probes. (f) Reactive ion etching ( $C_4F_8$ ,  $CHF_3$ ) is used to etch through the ONO layers, except where the wafer is covered with the photoresist. (g) The parts of the wafer not covered by the photoresist is etched from the upper ("device") layer by deep reactive ion etching (DRIE), down to the buried oxide layer, yielding probe profiles 100  $\mu m$  in thickness. (h) The existing photoresist is removed and a 2  $\mu m$  layer of Parylene-C is deposited over the entire device side of the wafer. Another layer of thick photoresist is deposited onto the device side. The device side of the wafer is bonded to a backing wafer (not shown in the drawing) in order to prepare for back-side etching by DRIE. (i) A layer of photoresist is spun onto the backside of the wafer and patterned. DRIE is performed from the backside of the wafer and the wafer is etched up to the buried oxide layer, which acts as an etch-stop for the DRIE. The buried oxide layer then is etched away by RIE, which does not etch Parylene and silicon. (j) Individual probes are removed from the wafer plane. (k) The tips of the probes are then shaped by mechanical grinding. (l) The residual Parylene and photoresist is removed from the probe and a new conformal layer of Parylene is deposited onto all surfaces, and the electrode sites and bonding pads are opened using an excimer laser. The Parylene-C residues are cleaned from the electrode sites and bonding pads in an oxygen plasma etcher. (k) Finally, iridium oxide is electroplated onto the active electrode sites.

## II: Work conducted at the House Ear Institute

### PABI Clinical Follow-up

Four PABI patients were seen in the second quarter of 2007: PABI 3, PABI#5, PABI#8 and PABI#9. PABI#3 has 4 penetrating microelectrodes that produce auditor percepts and PABI#9 has one. PABIs 5 and 8 use only their surface electrodes. PABI# 3 has very useable hearing remaining on his 2<sup>nd</sup> acoustic tumor side and therefore does not use his PABI on a daily basis. PABI #5 is still struggling with general health issues related to NF2 and also doesn't use his ABI on a daily basis. PABI #9 uses her PABI on a daily basis and has indicated a preference for her combination map which includes the penetrating electrode on which she receives auditory sensations.

With respect to patient performance, CUNY Sentence test scores using sound plus lipreading are 40% better than lipreading only for PABI #3, 15% better for PABI #5, 61% better for PABI#8, and 42% better for PABI #9. The actual %correct scores for each condition are presented in Table 1. This indicates that PABI sound can provide substantially improved communication ability over lipreading alone, even when the sound from the PABI alone is not adequate to allow word recognition.

Table 1

HINT Sentences	PABI Only	Lipreading	PABI+Lipreading
PABI 3 *	2	24	64
PABI 5	0	6	21
PABI 8	11	29	90
PABI 9 *	0	31	73

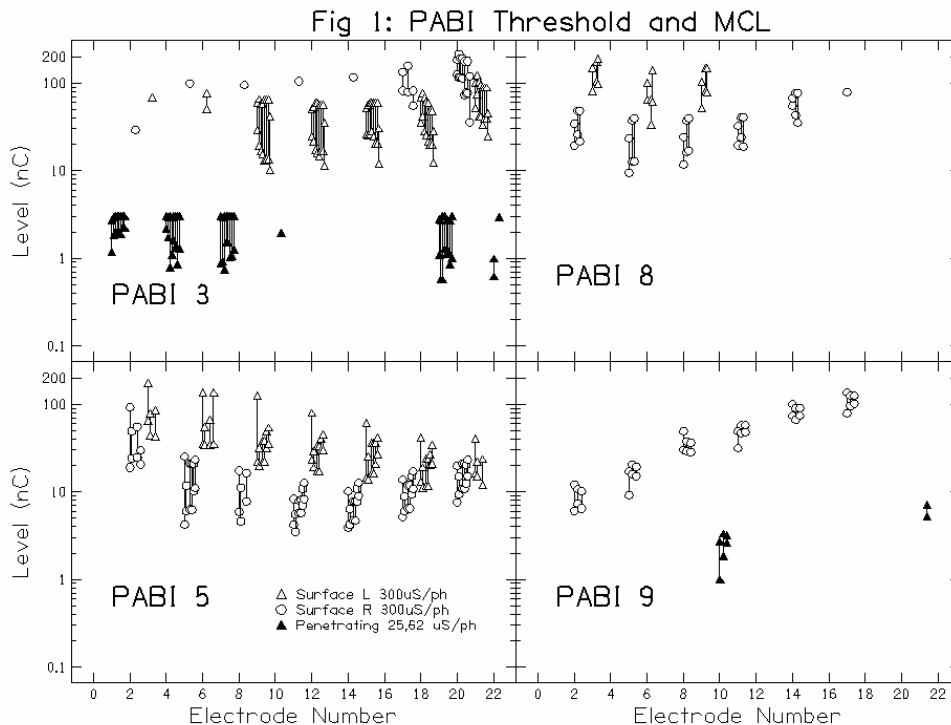
\* indicates use of penetrating electrodes in map

PABIs #3 and #9 have demonstrated benefits from combining penetrating electrodes with surface electrodes, however PABI #3 experiences only soft levels of auditory sensation on some of his penetrating electrodes at the charge limit. Therefore, with his combination map, there are some frequency regions that are not well covered in comparison with his surface electrode map. His useable surface electrodes all result in comfortably loud levels of sound, and therefore he does not experience any frequency regions of soft auditory sensation with this map. On some speech perception tests, his performance is better with his surface electrode program.

In general penetrating electrodes continue to show lower thresholds for electrical stimulation than surface electrodes, and with a range of pitch sensations. PABI #3 will require removal of his 2<sup>nd</sup> side acoustic tumor in all likelihood sometime in the next 6 months or so, at which time he will lose all remaining hearing in this ear and become totally reliant on his implant for hearing. His present performance is quite good with his PABI, and we expect that he, like previous patients in his situation, will find that his implant is very beneficial almost immediately.

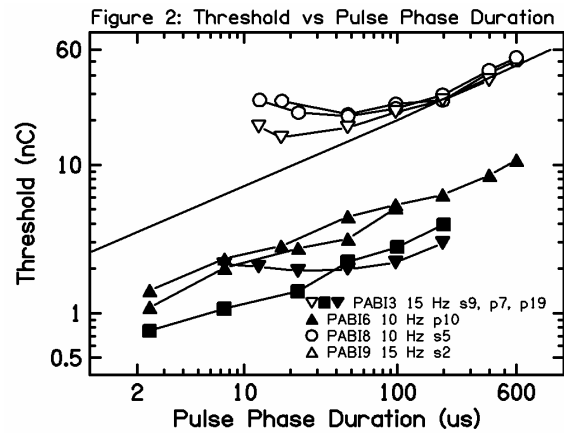
## Threshold and Dynamic Range Measures

Figure 1 presents threshold and most comfortable level (MCL) measures for the four PABI patients seen in this quarter. On each electrode threshold and MCL are connected by a vertical line. Successive measures are displaced slightly for clarity, with the rightmost set of points indicating the Threshold and MCL measures from the most recent measures. The two different open symbols represent measures on the two edges of the surface ABI electrode array, and the filled symbols present measures from the penetrating microelectrodes. Note that the levels measured on penetrating electrodes are significantly lower than those measured on surface electrodes. In general the lowest thresholds on surface electrodes are 3-10 nC, while threshold levels on penetrating electrodes were 1 nC or lower. In these four patients the electrodes along one side of the surface array produced lower thresholds than the other side, indicating a tilt of the surface electrode array with respect to the surface of the nucleus. In PABI9, electrodes along one side of the array provided auditory sensations while electrodes along the other edge did not. No systematic pattern of increasing or decreasing threshold levels was observed over time. Most electrodes showed stable threshold and MCL levels over time while a few showed increases or decreases in levels over time.



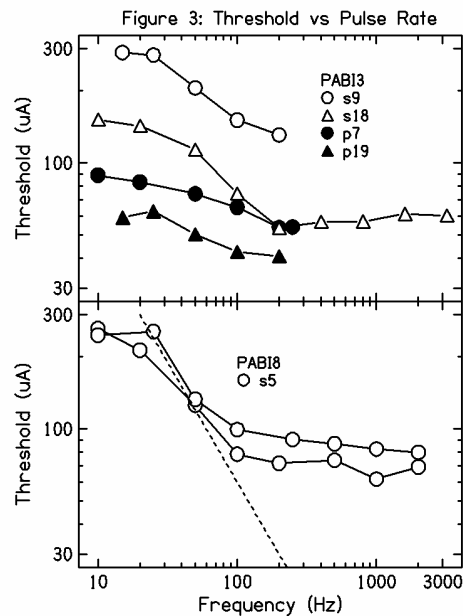
## Threshold as a Function of Pulse Phase Duration

Figure 2 presents measures on surface and penetrating electrodes of threshold levels as a function of the pulse phase duration. Penetrating electrodes (filled symbols) had lower thresholds than surface electrodes (open symbols) as expected. Thresholds typically decreased as pulse phase duration decreased, indicating more efficient use of charge for short phase durations. In some cases the threshold curves flattened out at short phase durations indicating a constant amount of charge at threshold for a range of pulse phase durations. The solid line indicates the function  $nC=kD^{0.75}$ , which is the function used to fit similar functions used by Zeng et al. (1998) to fit data from cochlear implant users. In this plot a constant amount of charge at threshold would be represented by a horizontal line. Some sections of the functions for surface electrodes and for penetrating electrode p19 for from PABI 3 are flat over part of the range. All other curves show decreasing charge as the pulse phase duration is decreased. The slope of these functions is similar to those observed by Zeng et al. in cochlear implants. This result is puzzling because the neurons in the cochlear nucleus are different in morphology, size, and function from primary auditory nerve fibers, yet their trade-off between current amplitude and pulse phase duration is similar.



### Threshold vs Pulse Rate

Figure 3 presents threshold measures as a function of the stimulating pulse rate for PABI 3 and PABI 8. Filled symbols show thresholds from penetrating electrodes and open symbols show thresholds from surface electrodes. The two curves shown for PABI 8 represent repeated measures after a 3-month interval and so indicate the test-retest reliability and stability over time of the measures. Note that in these two patients thresholds increase at low pulse rates for both surface and penetrating electrodes. The dashed line in the lower panel indicates perfect integration of the charge across multiple pulses. As the pulse rate increases, more pulses occur per unit of time and so a perfect integration of the charge across a time interval would result in lower thresholds. The threshold functions for PABI 8 are similar in slope to the perfect integration

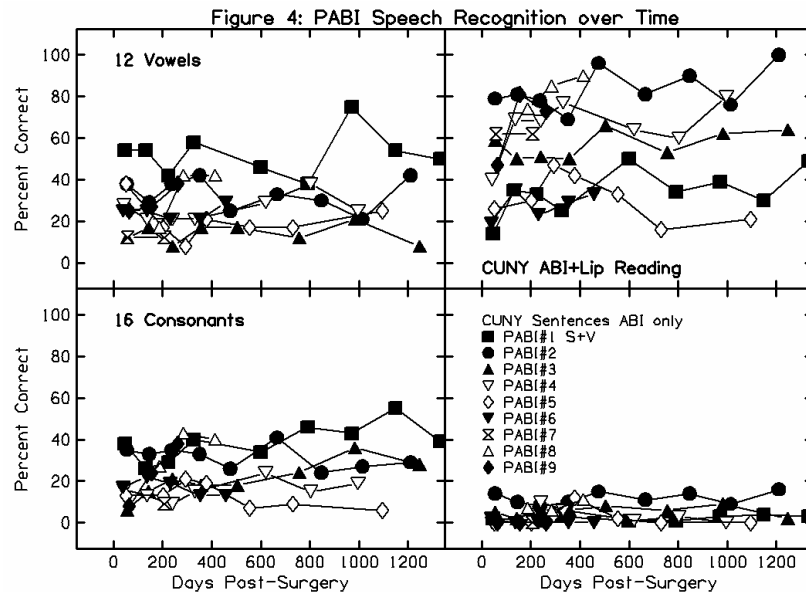


line while the functions from PABI 3 are considerably shallower than perfect integration. In both cases however, the increase in thresholds at low stimulation rates suggests an integration time constant on the order of 50 ms. Changing the stimulation rate from 20 Hz (50 ms between pulses) to 50 Hz (20 ms between pulses) results in a substantial decrease in threshold. Such long integration times are almost certainly not related to biophysical properties of the nerve and so must indicate more central integration of stimulation events. Threshold measures in cochlear implants show no change as a function of pulse rate between pulse rates of 10 to 200 Hz (e.g., Shannon, 1989).

### Speech Recognition Measures

Figure 4 presents speech discrimination and recognition measures over time. Patients who use penetrating electrodes in their speech processor are indicated by filled symbols, open symbols indicate patients who are only able to use surface electrodes in their speech processor maps.

Closed-set measures of vowel (12 alternatives) and consonant (16 alternatives) recognition were collected in sound-only mode (no lipreading). While there is some variability in these measures, there is no indication of improvements over time. Sentence



recognition (CUNY sentences) is presented both with lipreading (upper right panel) and using only the sound from the PABI device (lower right panel). Note that all patients are recognizing less than 20% correct in the sound only condition and show no improvement over time – up to 4 years of experience.

### Intra-operative Monitoring

During the last year, two patients (#9 and 10) were implanted with PABIs. In one case (#10), no successful intra-operative recordings of evoked potentials were made. No evoked potentials were seen for stimulation delivered through surface electrodes due to a technical error, and no recordings with stimulation through penetrating electrodes were attempted.

In the other case (#9), preliminary intra-operative recordings made with stimuli delivered through a handheld bipolar stimulating probe yielded at some locations evoked potentials identified as auditory brainstem responses (EABRs). After placement of the surface electrode array in the lateral recess, responses

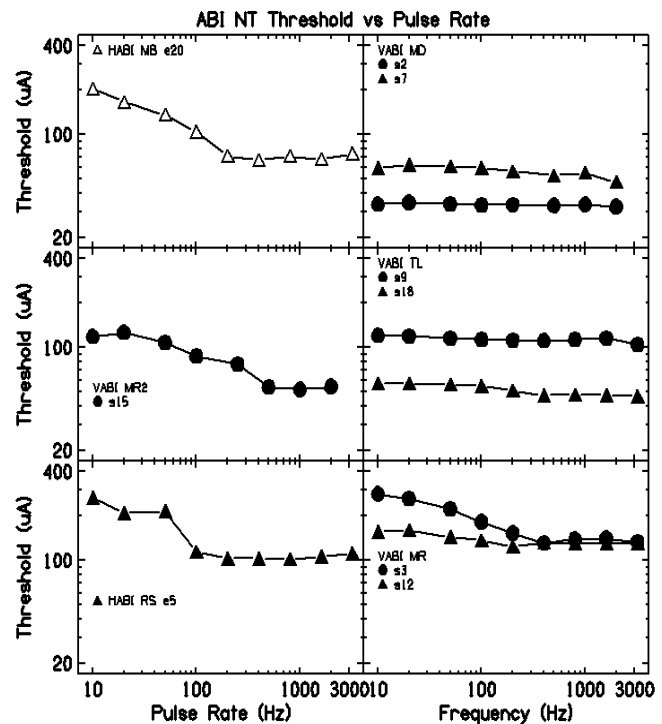
evoked by stimulating through surface electrodes were recorded that were identified as acceptable EABRs.

After insertion of the penetrating electrode array, recordings were made while stimulating between each needle electrode and the ball electrode placed under the Temporalis Muscle. The stimulus magnitude was 160  $\mu$ A, the maximum allowed for a 50  $\mu$ s phase duration of the biphasic pulses. Such stimulation resulted in evoked potentials of appreciable magnitude having waveforms similar to those of the preceding EABRs.

Discrepancies between these intra-operative monitoring results and the behavioral results obtained two months later at the initial stimulation session are puzzling. Although all ten penetrating electrodes had given similar response waveforms of various magnitudes, only two penetrating electrodes were found to be capable of evoking sound sensations. This is especially curious in view of the fact that all six electrodes in one row of surface electrodes were useful in evoking sound sensations, and those electrodes had given electrical responses with waveforms similar to the waveforms of the responses evoked with the penetrating electrodes. The origins of these discrepancies in these disappointing results are not known, but they may have to do with the fact that non-auditory sensations were evoked with all but one of the penetrating electrodes.

### Results from non-NF2 patients

Several patients with ABIs were tested in Italy and Germany in this quarter. The European patients have bilateral loss of their auditory nerves, but do not have NF2. Some of these non-tumor patients have been achieved high levels of open set speech recognition with the ABI. It is important to compare the speech and psychophysical results from this group of patients with surface electrodes with the performance of NF2 PABI patients. One measure collected in the last quarter was thresholds as a function of pulse rate. Figure 5 presents thresholds from 10Hz to more than 3000 Hz from 6 non-tumor ABI patients. Compare these results with the PABI data in Figure 3. The label HABI represents patients tested in Hannover and VABI are patients tested in Verona. Filled symbols represent results from patients who scored higher than 50% correct on recognition of sentences. Open symbols represent results from patients who



scored lower than 50% correct on sentence recognition testing. Note that two patterns of results were observed: flat curves showing little or no change in threshold as a function of pulse rate and curves that show rising thresholds at low stimulation rates. On the three patients where more than one electrode was measured, the threshold curves for the two electrodes were always of the same type, i.e. either both flat or both rising. This is similar to the results observed in the ABI patients with NF2. For each patient, all curves are of the same type, even between surface and penetrating electrodes. This suggests that the integration time implied by the rise at low stimulation rates is not electrode specific and is similar for surface and penetrating electrodes. Again, such a long integration time suggests that the mechanism is central.

### **References**

- Shannon, R.V. (1989). A model of threshold for pulsatile electrical stimulation of cochlear implants, *Hearing Research*, 40, 197-204.
- Zeng, F.-G., Galvin, J., and Zhang, C.-Y. (1998). Encoding loudness by electric stimulation of the auditory nerve, *NeuroReport*, 9(8), 1845-1848.